Superconductor Science and Technology

A new concept of a hybrid trapped field magnet lens

View the article online for updates and enhancements.

A new concept of a hybrid trapped field magnet lens

Keita Takahashi[1,3] ⬤, Hiroyuki Fujishiro[1] ⬤ and Mark D Ainslie[2] ⬤

[1] Department of Physical Science and Materials Engineering, Faculty of Science and Engineering, Iwate University, Morioka 020-8551, Japan
[2] Bulk Superconductivity Group, Department of Engineering, University of Cambridge, Cambridge CB2 1PZ, United Kingdom

E-mail: t2216017@iwate-u.ac.jp and fujishiro@iwate-u.ac.jp

CrossMark

Abstract

In this paper, a new concept of a hybrid trapped field magnet lens (HTFML) is proposed. The HTMFL exploits the 'vortex pinning effect' of an outer superconducting bulk cylinder, which is magnetized as a trapped field magnet (TFM) using field-cooled magnetization (FCM), and the 'diamagnetic shielding effect' of an inner bulk magnetic lens to generate a concentrated magnetic field higher than the trapped field from the TFM in the bore of the magnetic lens. This requires that, during the zero-field-cooled magnetization process, the outer cylinder is in the normal state ($T>$ superconducting transition temperature, T_c) and the inner lens is in the superconducting state ($T < T_c$) when the external magnetizing field is applied, followed by cooling to an appropriate operating temperature, then removing the external field. This is explored for two potential cases: (1) exploiting the difference in T_c of two different bulk materials ('case-1'), e.g. MgB_2 ($T_c = 39$ K) and GdBaCuO ($T_c = 92$ K) or (2) using the same material for the whole HTFML, e.g., GdBaCuO, but utilizing individually controlled cryostats, the same cryostat with different cooling loops or coolants, or heaters that keep the outer bulk cylinder at a temperature above T_c to achieve the same desired effect. The HTFML is verified using numerical simulations for 'case-1' using an MgB_2 cylinder and GdBaCuO lens pair and for 'case-2' using a GdBaCuO cylinder and GdBaCuO lens pair. As a result, the HTFML could reliably generate a concentrated magnetic field $B_c = 4.73$ T with the external magnetizing field $B_{app} = 3$ T in the 'case-1', and a higher $B_c = 13.49$ T with higher $B_{app} = 10$ T in the 'case-2', respectively. This could, for example, be used to enhance the magnetic field in the bore of a bulk superconducting NMR/MRI system to improve its resolution.

Keywords: hybrid trapped field magnet lens, bulk superconductors, trapped field magnets, magnetic lens, vortex pinning effect, diamagnetic shielding effect, finite element method

(Some figures may appear in colour only in the online journal)

1. Introduction

The superconducting characteristics of REBaCuO bulks (RE: rare earth element or Y) continue to be enhanced due to the

[3] Author to whom any correspondence should be addressed.

introduction of strong pinning centers and the improvement of crystal growth techniques, which have resulted in increased critical current density, J_c [1, 2]. As a result, such bulks exhibit higher trapped field capabilities using field-cooled magnetization (FCM) and have significant potential for practical applications as high-strength trapped field magnets (TFMs) capable of generating magnetic field of several Tesla. Figure 1(a) shows the time sequence of conventional FCM of superconducting bulks to utilize them as TFMs (the case shown is for a cylindrical ring bulk superconductor). Although the trapped field, B_T, of REBaCuO bulks, which can be estimated from the $J_c(B, T)$
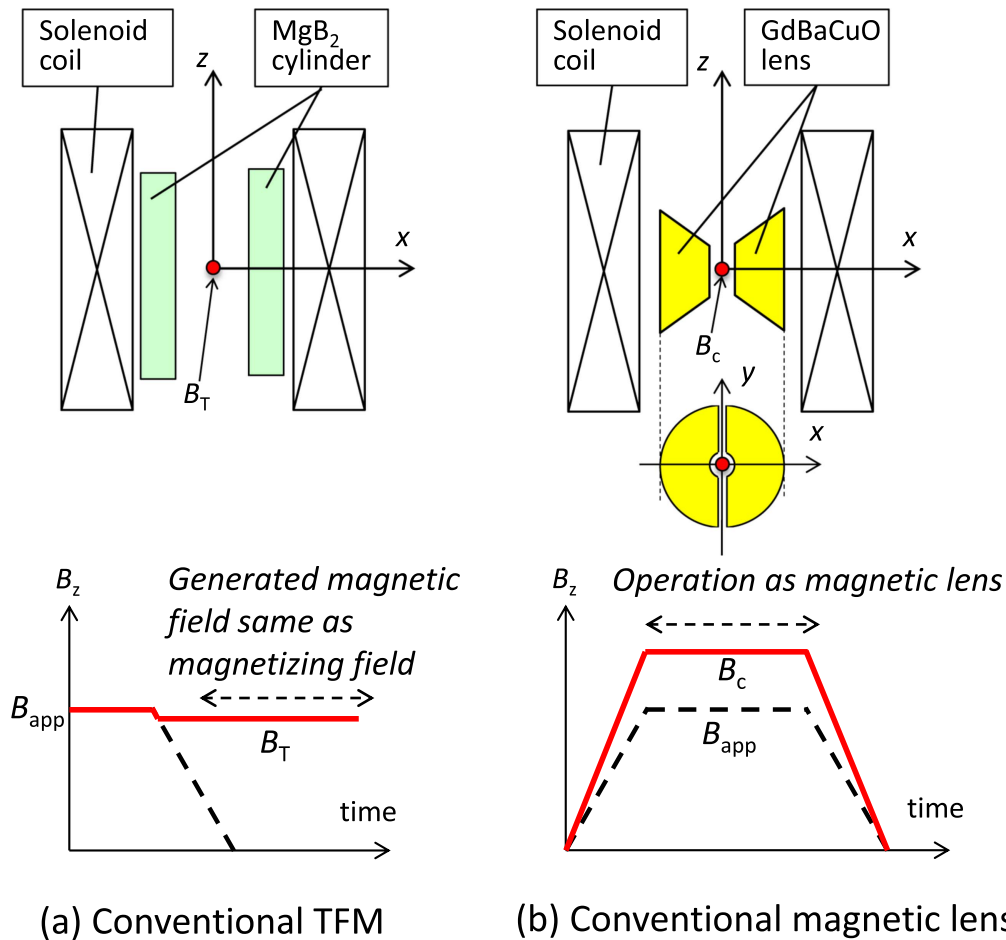
Figure 1. Time sequence of (a) conventional magnetizing process of field-cooled magnetization (FCM) of superconducting bulks to utilize them as TFMs and (b) magnetizing process of zero-field-cooled magnetization (ZFCM) for a conventional superconducting bulk magnetic lens.

characteristics, could be over 20 T at 20 K in a bulk pair [3], the mechanical strength of the brittle ceramic material restricts the practical maximum trapped field of such TFMs experimentally. To date, REBaCuO disk bulks have been shown to trap magnetic field over 17 T by mechanical reinforcement using glass fiber reinforced epoxy resin or shrink-fit stainless steel to reduce the electromagnetic hoop stress [3, 4]. Such TFMs, in which the field is trapped using the strong 'vortex pinning effect' of the material, require a high, stationary magnetic field to magnetize them and they can trap fields nearly the same or slightly lower than the applied field, B_{app}, using FCM, but such high fields are only available from specialized magnets at a limited number of facilities worldwide. In this sense, such high-strength TFMs are not practical for applications and much research been carried out on the pulsed field magnetization (PFM) technique as a fast, compact and relatively inexpensive magnetization technique. However, due to the large temperature rise associated with the rapid dynamic movement of the magnetic flux within the bulk, the trapped field capability is severely limited and only fields up to around 5 T have been achieved using PFM [5].

On the other hand, a 'magnetic lens' using cone-shaped superconducting bulks has been investigated, in which the magnetic flux is concentrated in the bore of the magnetic lens using the 'diamagnetic shielding effect' of superconducting materials and the available magnetic field in the lens is larger than

the applied field generated by the external magnetizing coil [6–9]. Figure 1(b) shows the time sequence of magnetizing process for a conventional bulk superconducting magnetic lens, for which zero-field-cooled magnetization (ZFCM) is used. The existence of slits in the superconducting hollow cone is essential to suppress the current along the circumferential direction and to concentrate the magnetic flux. A concentrated field of $B_c = 12.42$ T has been achieved at 20 K for a background field of $B_{app} = 8$ T using a bulk GdBaCuO magnetic lens [10] and $B_c = 30.4$ T has been achieved at the center of the lens in higher background field of $B_{app} = 28.3$ T elsewhere [11]. Using a bulk MgB$_2$ magnetic lens, a concentrated field of $B_c = 2.18$ T at 4.2 K has also been achieved for a background field of $B_{app} = 1$ T [12]. Mechanical reinforcement of the magnetic lens and the avoidance of the flux jump are necessary to achieve the magnetic lens effect stably [13]. Since the magnetic lens effect vanishes after the applied field decreased to zero, the external magnet must be operated continuously, which consumes a large amount of energy.

In this paper, we propose a new concept of a hybrid trapped field magnet lens (HTFML), consisting of a cylindrical bulk TFM using the vortex pinning effect, combined with a bulk magnetic lens using the diamagnetic shielding effect. The HTFML can reliably generate a magnetic field at the center of the magnetic lens higher than the trapped field in the single cylindrical bulk TFM and the external magnetizing field, even after the
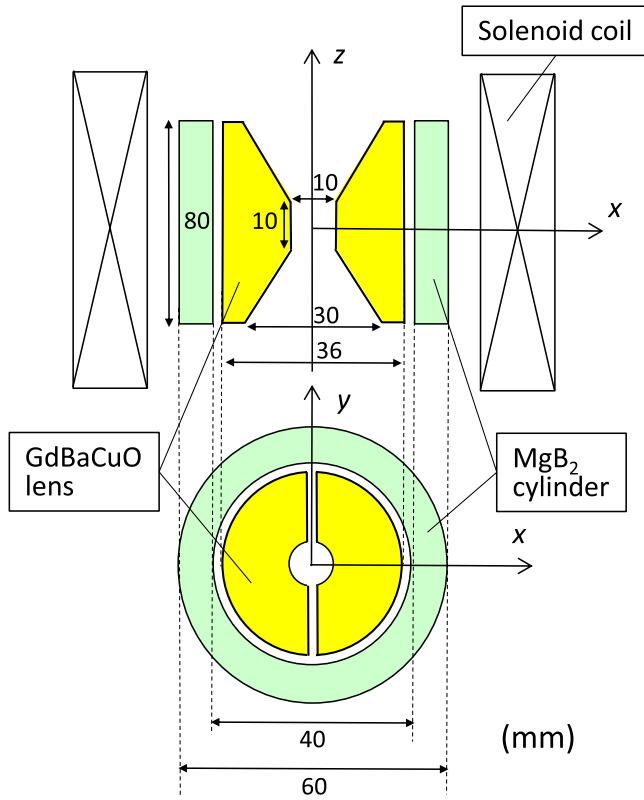
Figure 2. Numerical model and dimensions of the MgB$_2$ cylinder, GdBaCuO magnetic lens and solenoid magnetizing coil for 'case-1'. The MgB$_2$ cylinder is replaced by a GdBaCuO cylinder in 'case-2'.

externally applied field decreases to zero. This concept requires that, during the ZFCM process, the outer cylinder is in the normal state (T> superconducting transition temperature, T_c) and the inner lens is in the superconducting state ($T < T_c$) when the external magnetizing field is applied, followed by cooling to an appropriate operating temperature, then removing the external field. This is explored for two potential cases: (1) exploiting the difference in T_c of two different bulk materials ('case-1'), e.g. MgB$_2$ ($T_c = 39$ K) and GdBaCuO ($T_c = 92$ K) or (2) using the same material for the whole HTFML, e.g., GdBaCuO, but utilizing individually controlled cryostats, the same cryostat with different cooling loops or coolants, or heaters that keep the outer bulk cylinder at a temperature above T_c to achieve the same desired effect. The effectiveness and superiority of the HTFML is verified using numerical simulations for two cases: 'case-1' using an MgB$_2$ cylinder and REBaCuO lens pair, and 'case-2' using a REBaCuO cylinder and REBaCuO lens pair. The concentrated magnetic field in the HTFML changes depending on the superconducting characteristics of the bulks [14, 15], their shape and size [12], as well as the magnetizing conditions.

2. Numerical simulation framework

The following numerical simulation framework for the magnetizing process of the HTFML has been developed. A schematic view of the three-dimensional numerical model and the relevant dimensions are shown in figure 2, in which the

Table 1. Numerical parameters for the $J_c(B)$ characteristics of the bulk GdBaCuO material at 20 and 40 K using equation (2).

T (K)	J_{c1} (A m^{-2})	B_L (T)	J_{c2} (A m^{-2})	B_{max} (T)	α
40	3.5×10^9	0.9	2.7×10^9	6.0	0.8
20	9.0×10^9	1.5	5.4×10^9	8.0	0.5

superconducting cylinder is made from bulk MgB$_2$ and the superconducting magnetic lens is made from bulk GdBaCuO. This model is abbreviated as 'case-1'. The bulk MgB$_2$ cylinder is 60 mm in outer diameter (O.D.), 40 mm in inner diameter (I.D.) and 80 mm in height (H). The shape of the magnetic lens is referred from [13] so that the present numerical framework explains the concept of the HTFML based on such a typical lens geometry (as shown in figure 2), but importantly two slits exist that are 10° wide. The MgB$_2$ cylinder and GdBaCuO lens are magnetized by a solenoid coil of 170 mm in O.D., 120 mm in I.D. and 200 mm in H. Another example is also provided, in which both the superconducting cylinder and magnetic lens are made from bulk GdBaCuO, which is abbreviated as 'case-2'. The numerical simulation results for 'case-1' and 'case-2' are presented in sections 4.1 and 4.2, respectively.

Electromagnetic phenomena during the magnetization process are described by the fundamental equations shown elsewhere in detail [16–18]. The E–J power law is assumed to describe the nonlinear electrical properties of the superconducting bulk:

$$E = E_c \left(\frac{J}{J_c} \right)^n, \tag{1}$$

where E_c ($=10^{-4}$ V m^{-1}) is the characteristic electric field. $n = 20$ for the GdBaCuO bulk and $n = 100$ for the MgB$_2$ bulk are used [19]. The numerical simulation results depend strongly on the $J_c(B, T)$ characteristics of the superconductor [20–22]. For this study, the $J_c(B)$ characteristics for the GdBaCuO bulk are based on the equation presented by Jirsa *et al* to represent the so-called 'fish-tail' or 'peak' effect found in such superconducting materials [18, 23],

$$J_c(B) = J_{c1} \exp\left(-\frac{B}{B_L} \right) + J_{c2} \frac{B}{B_{max}} \exp\left[\frac{1}{\alpha} \left(1 - \left(\frac{B}{B_{max}} \right)^\alpha \right) \right]. \tag{2}$$

The values for the parameters J_{c1}, B_L, J_{c2}, B_{max} and α at 20 and 40 K used in the model are shown in table 1, respectively.

The $J_c(B)$ of the MgB$_2$ bulk is described by the following equation [24],

$$J_c(B) = J_{c0} \exp\left[-\left(\frac{B}{B_0} \right)^\beta \right], \tag{3}$$

where J_{c0}, B_0 and β are fitting parameters, which are summarized in table 2. Isothermal conditions are assumed while ramping down the field because the magnetization process is slow; hence, no thermal model is included.
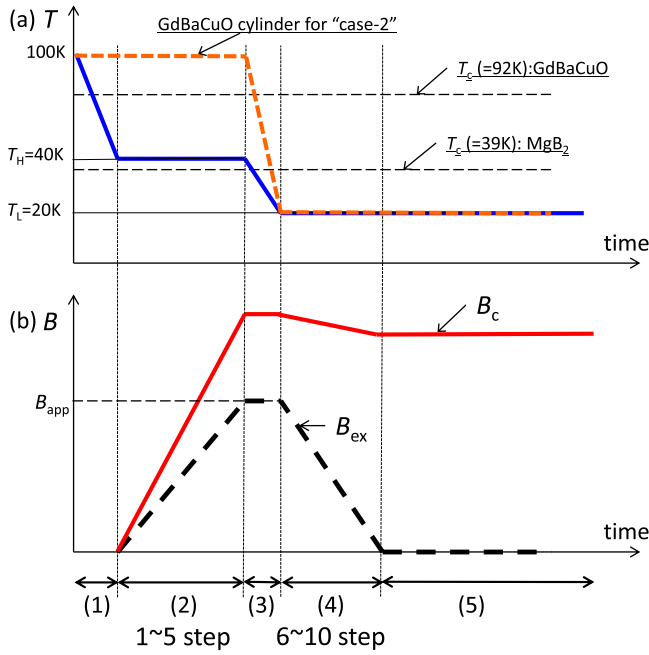
Figure 3. Time step sequence of (a) the temperature, T and (b) the external field, B_{ex}, and concentrated magnetic field, B_c, at the center of magnetic lens for 'case-1', in which an MgB$_2$ cylinder and GdBaCuO magnetic lens are used. In 'case-2', the temperature of the GdBaCuO lens follows the blue line and the GdBaCuO cylinder follows the dotted orange line in the upper panel (see text).

3. Magnetizing procedure

First, the magnetizing process is described for the following time step sequence, from (1) to (5), for the HTFML for 'case-1', in which the bulk MgB$_2$ cylinder and the bulk GdBaCuO magnetic lens are used. Figure 3 shows the time sequence of (a) the temperature, T and (b) the external field, B_{ex}, and concentrated magnetic field, B_c, at the center of the magnetic lens. The magnetizing applied field, B_{app}, corresponds to the maximum value of B_{ex}.

(1) The bulk MgB$_2$ cylinder and the bulk GdBaCuO lens are cooled from 100 K to $T_H = 40$ K, which is higher than the superconducting transition temperature of MgB$_2$, $T_c = 39$ K, but lower than that of GdBaCuO ($T_c = 92$ K). In this stage, the MgB$_2$ cylinder is in the normal state and the GdBaCuO lens is in the superconducting state (step 0).

(2) The external magnetic field, B_{ex}, is ramped up linearly at 0.222 T min^{-1} over five steps (steps 1–5) up to B_{app}, which corresponds to ZFCM of the GdBaCuO lens. The magnetic field, essentially higher than B_{app} because of the shielding effect by the magnetic lens, completely penetrates the MgB$_2$ cylinder and the magnetic field is concentrated at the center of the lens.

(3) The temperatures of both MgB$_2$ cylinder and GdBaCuO lens are then decreased to $T_L = 20$ K, which is lower than the T_c of MgB$_2$.

(4) B_{ex} is decreased linearly at 0.222 T min^{-1} over five steps (steps 6–10) down to zero. During this process,

Table 2. Numerical parameters for the $J_c(B)$ characteristics of the bulk MgB$_2$ material at 20 K using equation (3).

T (K)	J_{c0} (A m^{-2})	B_0 (T)	α
20	4.3×10^9	1.1	1.5

the MgB$_2$ cylinder is magnetized by FCM and magnetic flux is trapped in the cylinder. The magnetic field concentration effect slightly decreases due to the decrease of external field. However, a magnetic field at the center of the magnetic lens still remains due to the existence of the trapped field in the MgB$_2$ cylinder.

(5) As a result, HTFML can reliably generate a magnetic field higher than B_T of the single cylindrical TFM and B_{app}, even after $B_{ex} = 0$.

There are some examples of a practical cooling system using the difference in T_c of two superconducting components for an aircraft motor design [25] and a magnetic levitation application [26].

In 'case-2', in which both the superconducting cylinder and magnetic lens are made from bulk GdBaCuO, (1) and (2) above are changed as follows, labeled at (1') and (2'):

(1') The bulk GdBaCuO cylinder is maintained at 100 K (dotted orange line in figure 3) and the bulk GdBaCuO magnetic lens is cooled to $T_H = 40$ K (blue line in figure 3). Hence, the bulk GdBaCuO cylinder is in the normal state and the bulk GdBaCuO lens is in the superconducting state (step 0).

(2') The external magnetic field, B_{ex}, is increased linearly over five steps (steps 1–5) up to B_{app}, and the magnetic field, essentially equal to B_{app}, completely penetrates the GdBaCuO cylinder, but the GdBaCuO lens is magnetized by ZFCM.

In the next section, the results of the numerical simulation for 'case-1' and 'case-2' are presented to prove the effectiveness of the HTFML.

4. Simulation results and discussion

4.1. 'Case-1': MgB$_2$ cylinder–GdBaCuO lens

Figure 4 shows the time step dependence of the magnetic field profile along the x-direction across the center of the lens during (a) the ascending stage and (b) the descending stage of ZFCM of the GdBaCuO lens under an applied field, $B_{app} = 3$ T in 'case-1', which incorporates FCM of the MgB$_2$ cylinder. In figure 4(a), during the ascending stage from steps 0–5, the concentrated magnetic field, B_c, at the center of the GdBaCuO lens was enhanced with increasing B_{ex} owing to the diamagnetic shielding effect of the GdBaCuO lens. It can be found that there is little or no flux penetration in the GdBaCuO lens region ($r = \pm 5 \sim 18$ mm) in this case applying a relatively low magnetic field of 3 T by a magnetizing coil. The magnetic flux intrudes into the lens from inner
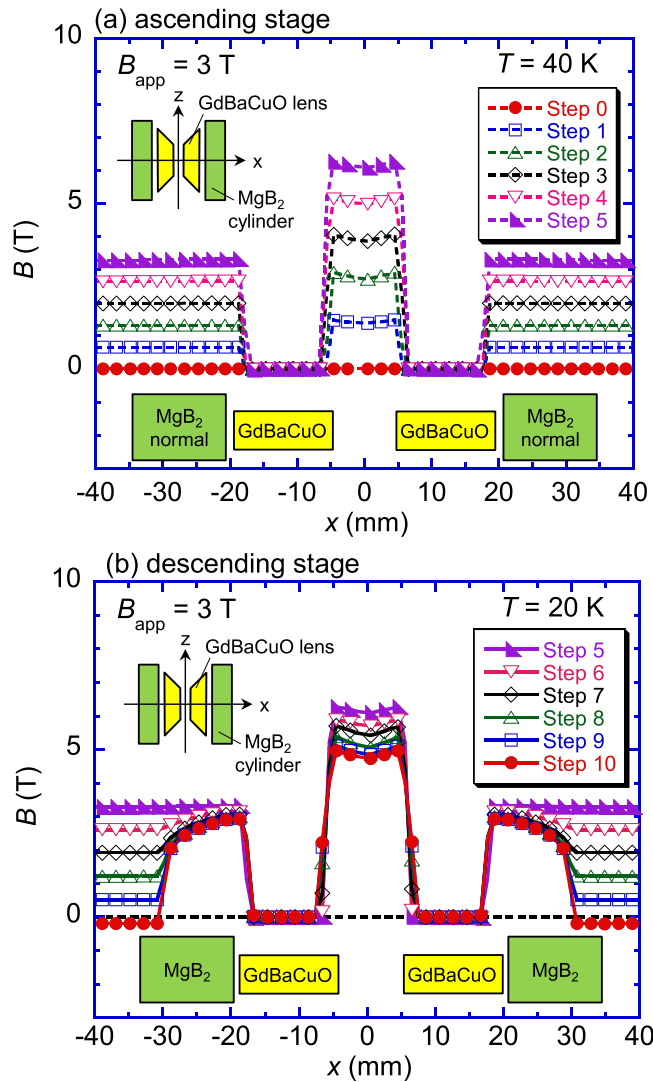
Figure 4. Time step dependence of the magnetic field profile along the *x*-direction across the center of the lens during (a) the ascending stage and (b) the descending stage of ZFCM of the GdBaCuO lens under an applied field, $B_{app} = 3$ T in 'case-1', which incorporates FCM of the MgB_2 cylinder.

Figure 5. Time step dependence of the magnetic field profile along the *x*-direction across the center of the lens during (a) the ascending stage and (b) the descending stage of FCM of the MgB_2 cylinder without the GdBaCuO lens for an applied field, $B_{app} = 3$ T at 20 K.

periphery rather than outer edge because of the magnetic flux concentration, which will be discussed later for higher B_{app} in 'case-2'. In this ascending stage, the GdBaCuO lens is under ZFCM conditions at 40 K; however, the MgB_2 cylinder is in the normal state and is not yet utilized as a TFM. In figure 4(b), during the descending stage of B_{ex} from steps 5–10, which incorporates FCM of the MgB_2 cylinder during ZFCM of the GdBaCuO lens, B_c decreased with decreasing B_{ex}, but becomes stable after the external field decreases to zero and a magnetic field is trapped in the MgB_2 cylinder. As a result, B_c at the center of the GdBaCuO lens settled to $B_c = 4.73$ T at the final step (step 10), which can be realized quasi-permanently by the novel combination of the 'vortex pinning effect' and 'diamagnetic shielding effect' of superconducting bulk materials.

Figures 5(a) and (b), respectively, show the time step dependence of the magnetic field profiles along the *x*-direction across the center of the lens during the ascending and
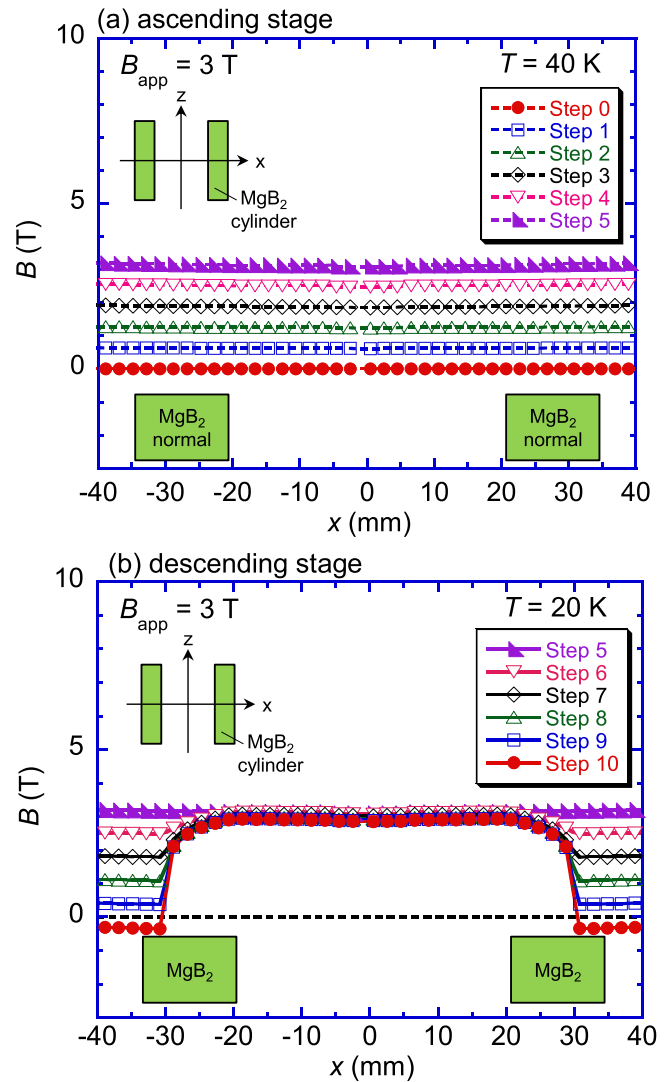
descending stages of FCM for an applied field, $B_{app} = 3$ T for only the MgB_2 cylinder, without the GdBaCuO lens, in 'case-1'. In figure 5(a), when only the MgB_2 cylinder is considered, the B_T value is nearly the same as B_{ex} in the ascending stage (steps 0–5), and attains a maximum value $B_{ex} = 3$ T at step 5 with a uniform magnetic field profile along *x*-direction, which corresponds to the applied field profile generated by the externally magnetizing coil. During this ascending stage, the MgB_2 cylinder is in the normal state. In figure 5(b), in the descending stage (steps 6–10), the trapped field, B_T, of the MgB_2 cylinder by FCM decreases slightly with decreasing B_{ex}, and settles to a final value of $B_T = 2.85$ T at the final step (step 10) in the bore of MgB_2 cylinder, now acting as a TFM that can continue to provide the trapped field quasi-permanently. One of the particular characteristics of the HTFML device is to utilize the trapped field from this TFM, instead of requiring a continuously applied field from an external magnetizing coil. Thus, it is useful to be able to reproduce a magnetic field profile similar to that which might be produced
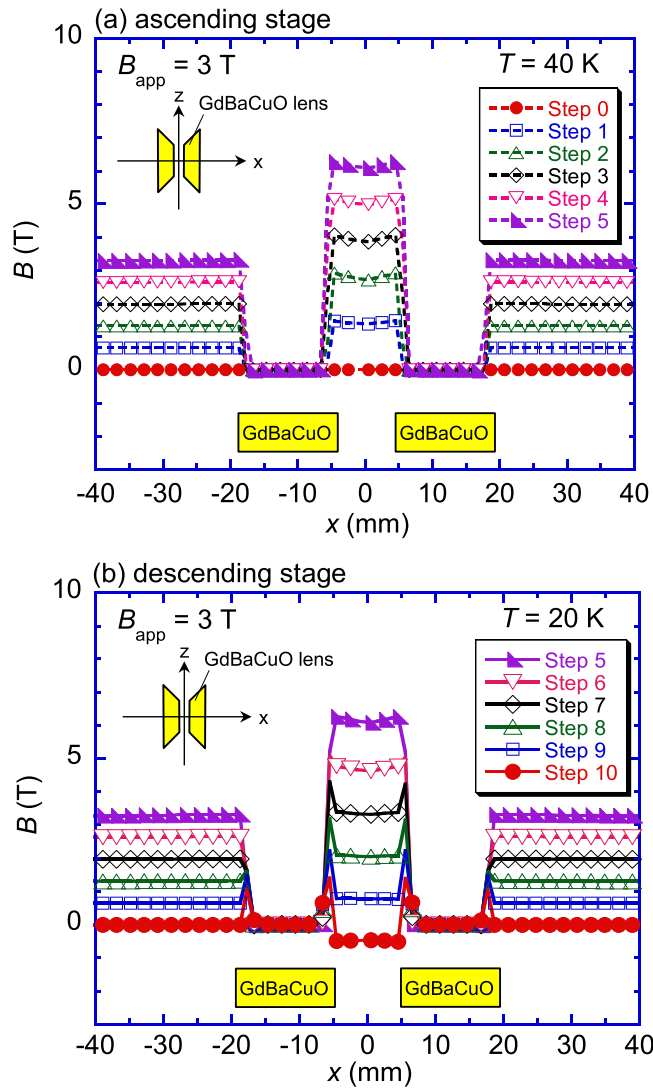
Figure 6. Time step dependence of the magnetic field profile along the *x*-direction across the center of the lens during (a) the ascending stage and (b) the descending stage of ZFCM of the GdBaCuO lens without the MgB$_2$ cylinder for an applied field, B_{app} = 3 T at 20 K.
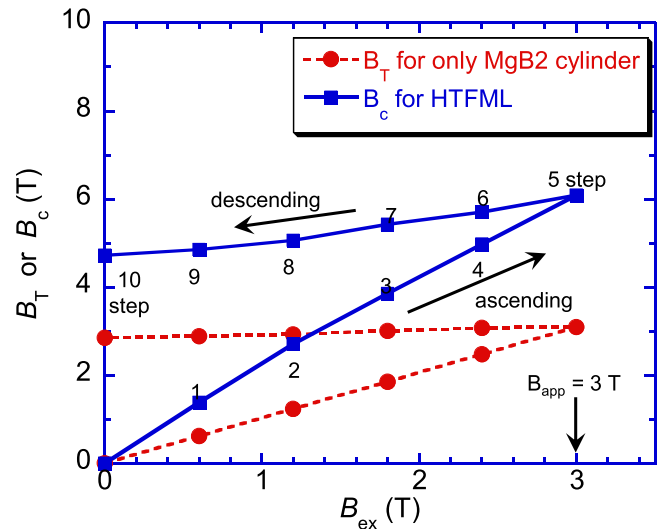

Figure 7. Concentrated magnetic field, B_c, at the center of the magnetic lens as a function of the external field, B_{ex}, for B_{app} = 3 T. The trapped field, B_T, at the center of the MgB$_2$ cylinder for the case without the GdBaCuO lens extracted from figure 5 is also shown.

by a magnetizing solenoid coil when we use the TFM as a source of magnetic field for the HTFML, for further concentration of the magnetic flux in the HTFML. This could, for example, allow the realization of higher resolution in a compact and cryogen-free NMR/MRI system using annular REBaCuO superconducting bulks [27, 28].

To achieve the highest concentrated field in the lens, the GdBaCuO magnetic lens must, in the ideal case, completely shield the magnetic field from its interior. However, since it is a type II superconductor, some magnetic flux will penetrate the material, depending on its $J_c(B, T)$ characteristics (and hence operating temperature), as well as its geometry, during the HTFML magnetizing procedure. Figures 6(a) and (b), respectively, show the time step dependence of the magnetic field profiles along the *x*-direction across the center of the lens during the ascending and descending stages of ZFCM for an applied field, B_{app} = 3 T for the only GdBaCuO lens without the MgB$_2$ cylinder in 'case-1'. Figure 6(a) is exactly the same

as figure 4(a), in which B_c at the center of the GdBaCuO lens was enhanced gradually with increasing B_{ex} in the ascending stage from steps 0–5. In figure 6(b), in the descending stage from steps 6–10, it can be seen that there is some flux penetration into the inner edge of GdBaCuO lens at around $r = \pm5 \sim 7$ mm from step 7 even for a relatively low applied field of 3 T during ZFCM. The magnetic field reached eventually becomes -0.46 T at the center of the GdBaCuO lens at the final step (step 10) after ZFCM, resulting in a reduction from the ideal of the GdBaCuO lens shielding effect in those regions where the magnetic flux penetrates during ZFCM. Thus, to maximize the lens's shielding, and hence its ability to concentrate the magnetic field, the flux penetration should be minimized.

Figure 7 shows the concentrated magnetic field, B_c, at the center of magnetic lens as a function of external field, B_{ex}, for B_{app} = 3 T, which was extracted from figure 4. The trapped field, B_T, at the center of the MgB$_2$ cylinder was also extracted from figure 5 for the case without the GdBaCuO lens, which clarifies the effectiveness of the HTFML. For only MgB$_2$ cylinder, the B_T value is nearly the same as B_{ex} in the ascending stage from step 0 and attains a maximum value B_{ex} = 3 T at step 5. The B_T value is then 2.85 T at the final step (step 10) once B_{ex} = 0, showing that 3 T is a reasonable value to fully magnetize the MgB$_2$ cylinder by FCM at 20 K. In the case of the HTFML using both the MgB$_2$ cylinder and GdBaCuO lens, B_c at the center of the GdBaCuO lens was enhanced up to 6.10 T at step 5 due to the shielding effect of lens and settled to B_c = 4.73 T at the final step (step 10), which is higher than both B_{app} from the magnetizing coil and B_T from the MgB$_2$ TFM. These results indicate the superiority of the proposed HTFML device, which can reliably generate the concentrated magnetic field higher than the applied field by the external magnetizing coil and the trapped field of the TFM, even after removal of the external field.
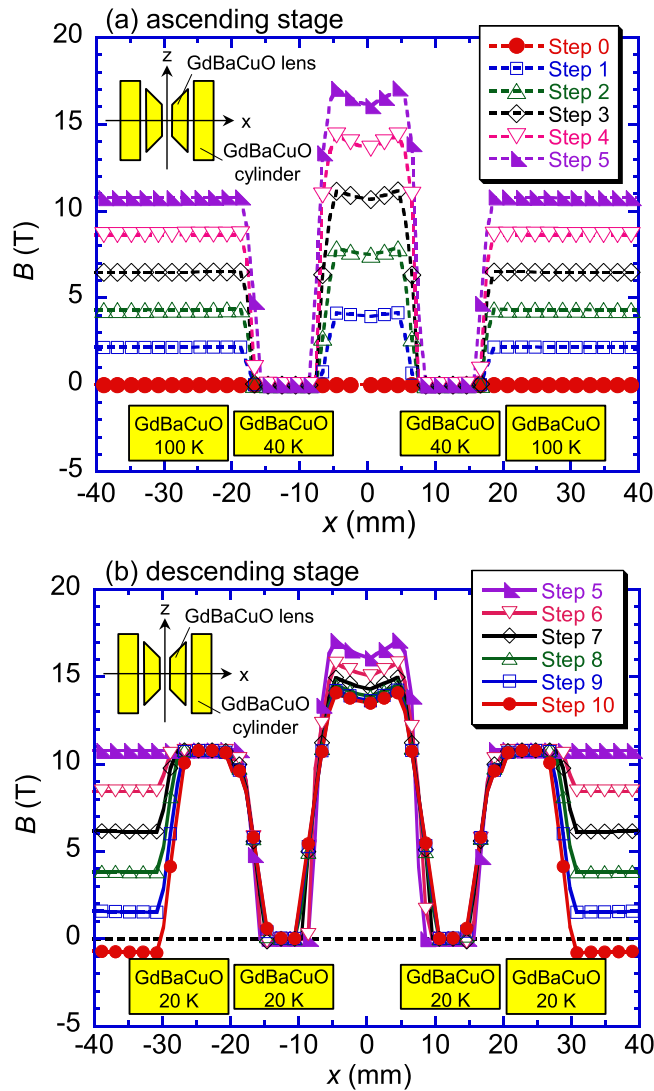
Figure 8. Time step dependence of magnetic field profile along the *x*-direction across the center of the lens during (a) the ascending stage and (b) the descending stage for $B_{app} = 10$ T in 'case-2'.

Figure 9. Time step dependence of the concentrated magnetic field, B_c, at the center of the GdBaCuO lens in the HTFML for $B_{app} = 3$, 6 and 10 T for 'case-2'. The external field, B_{ex}, generated by the solenoid magnetizing coil is also shown for each B_{app}.

4.2. 'Case-2': GdBaCuO cylinder–GdBaCuO lens

In the previous section, the superiority of the HTFML device in 'case-1' using a MgB$_2$ cylinder and REBaCuO lens pair was verified, for which the concentrated magnetic field was enhanced up to $B_c = 4.73$ T at the center of the GdBaCuO lens, which is higher than the trapped field of $B_T = 2.8$ T generated by the MgB$_2$ cylinder and the applied field, $B_{app} = 3.0$ T, generated by the external magnetizing coil. In this section, the other example of 'case-2' using a REBaCuO cylinder and REBaCuO lens pair for further concentration of the trapped magnetic flux is explored.

Figure 8 shows the time step dependence of the magnetic field profile along the *x*-direction across the center of the lens during (a) the ascending stage and (b) the descending stage for $B_{app} = 10$ T in 'case-2'. In this case, it should be noted that the temperature of the GdBaCuO cylinder and lens must be controlled individually. Similar results were shown previously for 'case-1' in figure 4(a), where the magnetic field profile was shown during the ascending stage of ZFCM for $B_{app} = 3$ T for
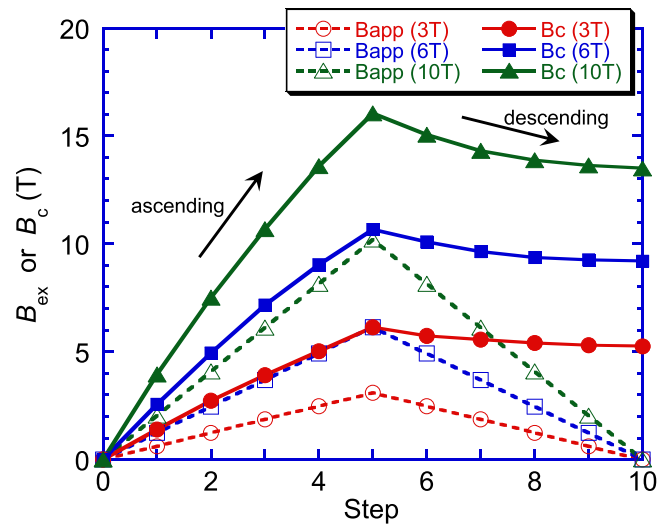
the GdBaCuO lens from steps 0–5 (noting that the MgB$_2$ cylinder is in the normal state). In figure 8(a), the B_c value was enhanced up to $B_c = 16$ T at the center of the lens at step 5 when applying $B_{app} = 10$ T. The GdBaCuO lens could retain its shielding effect even in a higher external magnetic field of 10 T, although the magnetic shielding effect weakens with increasing applied field due to further penetration of magnetic flux [11]. In figure 8(b), during the descending stage (steps 5–10), the GdBaCuO cylinder maintains a trapped field similar to B_{app} at the final step (step 10) as it is magnetized by FCM, but below its full capability based on its high J_c–B characteristics at 20 K. The B_c value gradually decreased during the descending stage and settled to a final value of $B_c = 13.5$ T at the center of the lens.

Figure 9 shows the time step dependence of the concentrated magnetic field, B_c, and external field, B_{ex}, at the center of the GdBaCuO lens for $B_{app} = 3$, 6 and 10 T for 'case-2'. Table 3 summarizes the concentrated magnetic field, B_c, trapped field from the TFM, B_T, when only considering the TFM cylinder (i.e., the lens is not present), at the central position at the final step (step 10), and the concentration ratio, B_c/B_{app}, in 'case-2' extracted from figure 9 for each actual B_{app}. An accurate value of B_{app} is shown as $B^*_{app} = 3.09$ T, 6.13 T and 10.18 T in this table, which was named roughly as $B_{app} = 3$, 6, 10 T so far. Similar results for 'case-1' from figure 4 are also shown for comparison. For the lower $B_{app} = 3$ T, a magnetic field concentration ratio of $B_c/B_{app} = 1.70$ is achieved at the final step (step 10) in 'case-2', which is higher than 1.53 when using the MgB$_2$ cylinder in 'case-1'. This results from the higher B_T value of 3.09 T in 'case-2', where the outside GdBaCuO cylinder was magnetized below its full capability. Furthermore, in 'case-2', the concentration ratio decreased with increasing B_{app} from 1.70 for $B_{app} = 3$ T to 1.33 for $B_{app} = 10$ T. In figure 9, the higher B_{app} resulted in a larger flux creep during the descending stage of FCM of the TFM cylinder and further penetration of magnetic flux in the ZFCM of the GdBaCuO lens. There is a possibility to achieve further

Table 3. Concentrated magnetic field, B_c, trapped field by TFM, B_T, at the center of the GdBaCuO lens at the final step (step 10), and magnetic field concentration ratio, B_c/B_{app}, in 'case-2' extracted from figure 9 for each actual applied field, B^*_{app}. Similar results for 'case-1' from figure 4 are also shown for comparison.

	B_{app} (T)	B^*_{app} (T)	B_T (T)	B_c (T)	B_c/B_{app}
'case-1' (MgB2 cylinder)	3	3.09	2.85	4.73	1.53
'case-2' (GdBaCuO cylinder)	3	3.09	3.09	5.25	1.70
	6	6.13	6.13	9.19	1.50
	10	10.18	10.18	13.49	1.33

enhancement of B_c and B_c/B_{app} by optimization of the magnetic design, including the geometry of the cylinder and lens, and the magnetization conditions, including temperature and applied field. The shielding property of the magnetic lens should be also exploited for further concentration of the trapped field, such as for hollow bulk cylinders [14]. These results show that the effectiveness of the HTFML would be enhanced in terms of the characteristics of the superconducting material(s) used, including the possibility of utilizing new and improved materials, such as $BaFe_2As_2$ ($T_c = 38$ K) [29, 30].

5. Conclusion

A new concept of an HTFML, consisting of a superconducting bulk cylinder TFM using the vortex pinning effect, combined with a bulk magnetic lens using the diamagnetic shielding effect, is proposed, which can reliably generate a magnetic field at the center of the magnetic lens higher than the trapped field by TFM and the maximum external magnetizing field, even after the externally applied field decreases to zero. The effectiveness and superiority of the HTFML was verified using numerical simulations for two examples: (1) an MgB_2 cylinder and GdBaCuO lens pair ('case-1') and (2) a GdBaCuO cylinder and GdBaCuO lens pair ('case-2'). In 'case-1', using the outer MgB_2 cylinder and inner GdBaCuO lens pair, the MgB_2 cylinder was magnetized by FCM with an applied field, $B_{app} = 3$ T, during the descending stage, also corresponding to ZFCM of the GdBaCuO lens. The trapped field, $B_T = 2.85$ T, in the MgB_2 TFM cylinder was concentrated by the introduction of GdBaCuO lens, and a concentrated magnetic field, $B_c = 4.73$ T, was reliably achieved at the center of the lens. In 'case-2', using the outer GdBaCuO TFM cylinder and inner GdBaCuO lens pair, in which the GdBaCuO cylinder is held above T_c and the GdBaCuO lens is cooled below T_c for the ascending stage of magnetization, followed by both bulks being cooled below T_c for the descending stage, a higher $B_c = 13.49$ T, was reliably achieved at the center of the magnetic lens for $B_{app} = 10$ T.

The advantages and disadvantages of each HTFML, comparing use of the MgB_2 cylinder and the GdBaCuO cylinder are summarized as follows:

'case-1': The MgB_2 HTFML only needs one cooling process for the whole device by exploiting the difference in T_c of the two superconducting materials. Its weight would also be lower due to the use of the lighter bulk MgB_2 cylinder. However, the trapped field capability is limited in comparison to the GdBaCuO cylinder ('case-2') because of the comparatively inferior $J_c(B)$ characteristics of MgB_2 and it must operate at a temperature lower than the superconducting transition temperature of MgB_2, $T_c = 39$ K.

'case-2': The all-GdBaCuO HTFML offers higher concentrated fields at temperatures much higher than 39 K, but does require separate cooling of the cylinder and lens parts to obtain the necessary effect and it would weigh more.

This HTFML device could become a standard method for trapped field enhancement in several practical applications using a superconducting bulk and there is a scope for optimization of the magnetic design, including geometry around two bulks, and magnetization conditions, including temperature and applied field. The effectiveness of the HTFML would be enhanced with improvements in the characteristics of the superconducting material(s) used, including the possibility of utilizing new and improved materials such as $BaFe_2As_2$ ($T_c = 38$ K). The device could, for example, be used to enhance the magnetic field in the bore of a bulk superconducting NMR/MRI system to improve its resolution.

ORCID iDs

Keita Takahashi ⬤ https://orcid.org/0000-0002-8278-2688
Hiroyuki Fujishiro ⬤ https://orcid.org/0000-0003-1483-835X
Mark D Ainslie ⬤ https://orcid.org/0000-0003-0466-3680

References

[1] Shi Y-H, Namburi D K, Zhao W, Durrell J H, Dennis A R and Cardwell D A 2016 *Supercond. Sci. Technol.* **29** 015010
[2] Muralidhar M, Sakai N, Chikumoto N, Jirsa M, Machi T, Nishiyama M, Wu Y and Murakami M 2002 *Phys. Rev. Lett.* **89** 237001
[3] Tomita M and Murakami M 2003 *Nature* **421** 517–20

[4] Durrell J H *et al* 2014 *Supercond. Sci. Technol.* **27** 082001
[5] Fujishiro H, Tateiwa T, Fujiwara A, Oka T and Hayashi H 2006 *Physica* C **334–338** 445–8
[6] Matsumoto S, Kiyoshi T, Asano T, Ozaki O, Koyanagi K, Fujihira J and Wada H 2003 *IEEE Trans. Appl. Supercond.* **13** 1652–5
[7] Matsumoto S, Asano T, Kiyoshi T and Wada H 2004 *IEEE Trans. Appl. Supercond.* **14** 1666–9
[8] Asano T, Itoh K, Matsumoto S, Kiyoshi T, Wada H and Kido G 2005 *IEEE Trans. Appl. Supercond.* **15** 3157–60
[9] Kiyoshi T, Choi S, Matsumoto S, Asano T and Uglietti D 2009 *IEEE Trans. Appl. Supercond.* **19** 2174–7
[10] Zhang Z Y, Matsumoto S, Teranishi R and Kiyoshi T 2012 *Supercond. Sci. Technol.* **25** 115012
[11] Choi S, Yoon J-H, Lee B-S, Won M-S, Ok J-W, Zhang Z-Y, Kiyoshi T, Matsumoto S and Lee S-H 2012 *J. Appl. Phys.* **111** 07E728
[12] Zhang Z Y, Choi S, Matsumoto S, Teranishi R, Giunchi G, Albisetti A F and Kiyoshi T 2012 *Supercond. Sci. Technol.* **25** 025009
[13] Zhang Z Y, Matsumoto S, Teranishi R and Kiyoshi T 2013 *Supercond. Sci. Technol.* **26** 045001
[14] Lousberg G P, Fagnard J F, Ausloos M, Vanderbemden P and Vanderheyden B 2010 *IEEE Trans. Appl. Supercond.* **20** 33–41
[15] Rabbers J J, Oomen M P, Bassani E, Ripamonti G and Giunchi G 2010 *Supercond. Sci. Technol.* **23** 125003
[16] Fujishiro H and Naito T 2011 *Supercond. Sci. Technol.* **23** 105021
[17] Fujishiro H, Ainslie M D, Takahashi K, Naito T, Yanagi Y, Itoh Y and Nakamura T 2017 *Supercond. Sci. Technol.* **30** 085008
[18] Takahashi K, Fujishiro H, Naito T, Yanagi Y, Itoh Y and Nakamura T 2017 *Supercond. Sci. Technol.* **30** 115006
[19] Fujishiro H, Naito T and Yoshida T 2014 *Supercond. Sci. Technol.* **27** 065019
[20] Ainslie M D, Zou J, Mochizuki H, Fujishiro H, Shi Y-H, Dennis A R and Cardwell D A 2015 *Supercond. Sci. Technol.* **28** 125002
[21] Ainslie M D and Fujishiro H 2015 *Supercond. Sci. Technol.* **28** 053002
[22] Ainslie M D, Zhou D, Fujishiro H, Takahashi K, Shi Y-H and Durrell J H 2016 *Supercond. Sci. Technol.* **29** 124004
[23] Jirsa M, Půst L, Dlouhý D and Koblischka M R 1997 *Phys. Rev.* B **55** 3276–84
[24] Xiang F X, Wang X L, Xun X, Silva K S B D, Wang Y X and Dou S X 2013 *Appl. Phys. Lett.* **102** 152601
[25] Masson P J, Breschi M, Tixador P and Luongo C A 2007 *IEEE Trans. Appl. Supercond.* **17** 1533–6
[26] Patel A, Giunchi G, Albisetti A F, Shi Y, Hopkins S C, Palka R, Cardwell D A and Glowacki B A 2012 *Phys. Proc.* **36** 937–42
[27] Nakamura T, Tamada D, Yanagi Y, Itoh Y, Nemoto T, Utsumi H and Kose K 2015 *J. Magn. Reson.* **259** 68–75
[28] Ogawa K, Nakamura T, Terada Y, Kose K and Haishi T 2011 *Appl. Phys. Lett.* **98** 234101
[29] Weiss J D, Yamamoto A, Polyanskii A A, Richardson R B, Larbalestier D C and Hellstrom E E 2015 *Supercond. Sci. Technol.* **28** 112001
[30] Ainslie M D, Yamamoto A, Fujishiro H, Weiss J D and Hellstrom E E 2017 *Supercond. Sci. Technol.* **30** 105009